

Relationship between Conformational Dynamics and Electron Transfer in a Desolvated Peptide. Part I. Structures

David Semrouni, Carine Clavaguéra,* and Gilles Ohanessian*

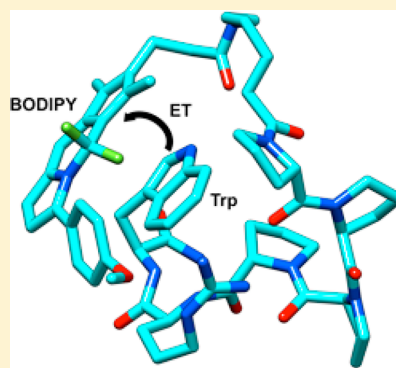
Laboratoire des Mécanismes Réactionnels, Department of Chemistry, Ecole Polytechnique, CNRS, 91128 Palaiseau Cedex, France

Joel H. Parks*

Rowland Institute at Harvard, 100 Edwin H. Land Boulevard, Cambridge, Massachusetts 02142, United States

S Supporting Information

ABSTRACT: The structures, dynamics and energetics of the protonated, derivatized peptide DyeX-(Pro)₄-Arg⁺-Trp, where “Dye” stands for the BODIPY analogue of tetramethylrhodamine and X is a (CH₂)₅ linker, have been investigated using a combination of modeling approaches in order to provide a numerical framework to the interpretation of fluorescence quenching data in the gas phase. Molecular dynamics (MD) calculations using the new generation AMOEBA force field were carried out using a representative set of conformations, at eight temperatures ranging from 150 to 500 K. Force field parameters were derived from ab initio calculations for the Dye. Strong electrostatic, polarization and dispersion interactions combine to shape this charged peptide. These effects arise in particular from the electric field generated by the charge of the protonated arginine and from several hydrogen bonds that can be established between the Dye linker and the terminal Trp. This conclusion is based on both the analysis of all structures generated in the MD simulations and on an energy decomposition analysis at classical and quantum mechanical levels. Structural analysis of the simulations at the different temperatures reveals that the relatively rigid polyproline segment allows for the Dye and Trp indole side chain to adopt stacking conformations favorable to electron transfer, yielding support to a model in which it is electron transfer from tryptophan to the dye that drives fluorescence quenching.



1. INTRODUCTION

Fluorescence-based methods have been developed to probe the structure and local conformational dynamics of trapped gas-phase biomolecule ions which have been derivatized with a strongly fluorescing dye. Measurements have included quenching in Trp-cage protein,^{1,2} polyproline peptide sequences,^{3,4} and noncovalent Vancomycin-peptide complexes.⁵ In each case the quenching could be related to conformational changes with temperature induced by spatial fluctuations of the side chains. Experiments verified that interactions between the dye and a Trp residue were required to observe quenching of the dye fluorescence.

Measurements of the unsolvated peptide sequences of DyeX-(Pro)_n-Arg⁺-Trp, where “Dye” stands for the BODIPY (boron-dipyrromethene class of dye) analogue of tetramethylrhodamine and X is a (CH₂)₅ linker (see Scheme 1), introduced a unique opportunity to study the quenching process, since these sequences constrain fluctuations except for the interacting dye and Trp side chain.^{3,4} This paper (part I) concentrates on a detailed structural analysis of the peptide sequence DyeX-(Pro)₄-Arg⁺-Trp as a function of temperature including both molecular dynamics (MD) and density functional theory (DFT) calculations. The calculated temperature dependence of conformational fluctuations are derived from MD calcu-

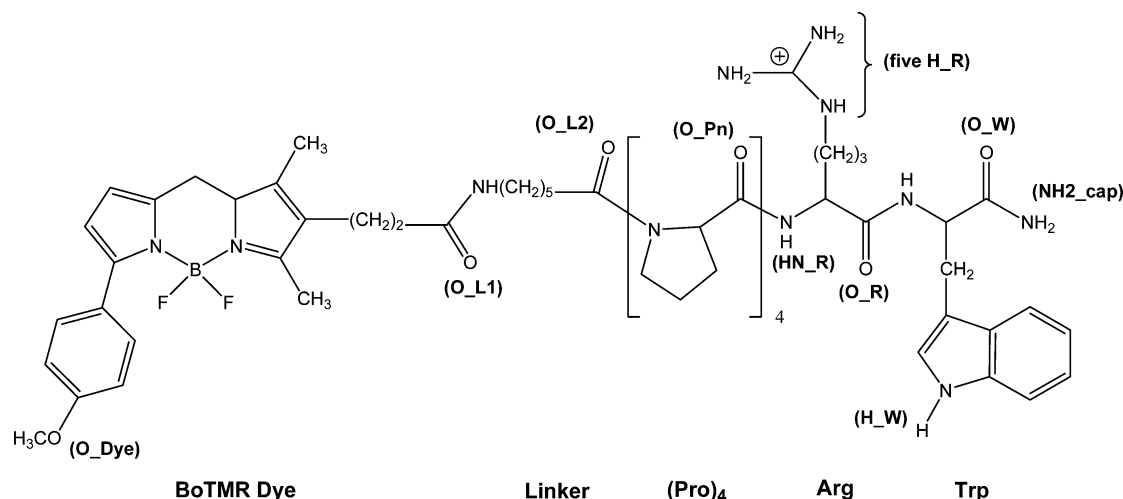
lations in the following paper (part II²⁸) to compare the quenching rate data with the temperature dependence of the Marcus model of the electron transfer rate. These structure calculations not only allow us to identify conformations exhibiting Dye-Trp proximity and exothermic reactivity required for rapid quenching by electron transfer, but also provide a detailed description of the intramolecular interactions responsible for the occurrence of such quenching conformations.

This effort to identify the basis for fluorescence lifetime quenching in biomolecules is required to understand if such measurements can yield fundamental information related to changes in properties such as conformation. In general, the probability of electron transfer in biomolecules has been shown to be intimately dependent on the conformation through the local separation of the electron donor and acceptor. Consequently, to the extent that fluorescence lifetime quenching is a consequence of electron transfer interactions, quenching data will display the signature of local changes in conformation. The capability to isolate local changes within a

Received: August 7, 2012

Revised: December 12, 2012

Published: January 8, 2013

Scheme 1. Detailed Labeling of the Sequence DyeX-(Pro)₄-Arg⁺-Trp

biomolecular conformation offers the possibility of identifying dynamic changes occurring within specific regions of secondary structure. These gas-phase methods also have the advantage that measurements can be directly related to DFT calculations and MD simulations. An understanding of the dynamics derived from intramolecular interactions in the absence of surrounding water layers provides a basis for exploring changes in these dynamics introduced in condensed phase measurements.

Previous molecular dynamics calculations⁴ performed to identify the basis for the fluorescence quenching were consistent with an electron transfer process but did not provide an unambiguous result that confirmed the presence of electron transfer. This paper presents the analysis of MD simulations of the structural fluctuations for an unsolvated peptide sequence DyeX-(Pro)₄-Arg⁺-Trp. These simulations are based on the new generation AMOEBA force field,^{5–12} which explicitly includes polarizability contributions as well as atomic multipole-based electrostatic interactions and a refined van der Waals term. This is expected to bring higher reliability to MD results and improved ability to identify the crucial energy terms, especially when strong local electrostatic, polarization and dispersion interactions are expected. This is particularly relevant for calculations of a charged, unsolvated peptide in which multiple hydrogen bonds and π -stacking interactions are likely to occur. These calculations determined the intramolecular interactions contributing to formation of the peptide conformations and the forces driving the conformational fluctuations. In particular, the MD trajectories displayed fluctuations among conformers which varied in the separation of the dye and Trp residue as a function of temperature. Since electron transfer interactions depend exponentially on this separation, this parameter serves to identify correlations between the temperature dependence of the electron transfer rate and the quenching rate. In addition, DFT calculations were performed on several structures identified in the MD simulations. Reliable quantum chemical results for systems of this level of complexity are not commonly available in the literature. The DFT interaction energy between molecular fragments was further decomposed into components following the Morokuma–Ziegler¹³ scheme in order to strengthen the identification of energy terms at work in a π -stacking interaction between the dye and Trp side chain. The results

underline the requirements for a force field to properly model the forces which are responsible for the formation of these conformations that are critical for electron transfer.

2. COMPUTATIONAL METHODS

2.1. Force Field. Force fields whose electrostatic energy component is based only on point charges have been shown to reproduce only half of a set of amino acid conformations as established by accurate quantum chemical calculations, whereas the new generation force field AMOEBA reaches 80% of reproduction.^{7,14} For the derivatized peptide studied herein, the presence of the charged Arg side chain and aromatic rings in both Trp side chain and the BODIPY suggests a special importance of electrostatics and polarization in structures, energetics and a fortiori dynamics. The fluorescence quenching model via electron transfer⁴ involves the Dye and the Trp side chain. For a correct description of interactions between those two groups in the presence of a charged Arg residue, one needs to calculate polarization which is nonadditive by nature. For this purpose, we have used the AMOEBA force field, developed by Ren and Ponder.^{6,9–11} Polarization is calculated through mutually induced point dipoles¹⁵ damped according to a Thol  model.¹⁶ The calculation of electrical interactions is based on atomic induced dipole sites and on permanent atomic charges, dipoles and quadrupoles. In addition, dispersion is important for describing the local interactions of aromatic cycles and for peptide folding in general.¹⁷ AMOEBA uses a “buffered 14–7” functional form, instead of a classical Lennard-Jones function, to improve the modeling of van der Waals interactions.¹⁸ All AMOEBA calculations have been performed with the Tinker package version 5.0.⁸

2.2. Dye Parameters. AMOEBA parameters were available for peptide residues and terminal caps but not for the linker and the Dye. The linker was mainly assimilated to a lysine CH₂ chain terminated by two peptidic amides. We consider the same simplification of the BODIPY as used in previous studies:⁴ the replacement of a B–N atom pair by two carbons. The Dye C₆H₄-O-CH₃ group is considered as a Tyr side chain modified to be a methyl ether. The OCH₃ parameters are those of the methyl ether defined in AMOEBA. Corresponding van der Waals parameters exist in AMOEBA parameter sets for proteins and organic molecules.¹⁰ The three rings of BODIPY needed more parameter adaptation. Approximation was made on

torsion parameters in the Dye, considering them to be null because of the strong planarity preference of aromatic rings. For C, N, and H atoms involved in aromatic cycles we used van der Waals parameter values available for other aromatic cycles. In AMOEBA, fluorine is defined as a fluoride ion. van der Waals parameters were consequently taken from the Merck force field¹⁸ which uses the same potential formulation for van der Waals interactions. Atomic polarizabilities were already defined for each element and therefore taken from available AMOEBA parameter sets.

For electrostatic parameter determination, quantum mechanics was used in order to be consistent with its treatment in standard AMOEBA. Multipoles were extracted via Stone's distributed multipole algorithm (DMA)¹⁹ as implemented in the GDMA 2.2 software.²⁰ In order to remain consistent with existing AMOEBA multipoles, DMA was applied to a wave function calculated with the MP2 method associated with the cc-pVTZ basis set, using the initial algorithm. A computation at this level was not performed on the whole Dye but rather on the three rings only, replacing methyl and other substituents, except for fluorine, by hydrogen atoms. As for some other chemical groups, methyls linked to an aromatic cycle are already defined in AMOEBA and we have considered their parameters to be transferable. Charge, dipole and quadrupole parameters for the atoms of the three rings of the Dye are derived from DMA calculations performed with a H radius of 0.31 Å. After reintroducing the three rings in the whole system, the total charge has been set to its correct integer value by small modifications of atom partial charges.

2.3. Starting Structures and MD Calculations. The AMOEBA force field including new atom types and parameters for BODIPY as described above was used to calculate the potential energy during MD trajectories. These simulations have been performed at several temperatures using a Berendsen thermostat (coupling time: 0.1 ps). Trajectories were propagated by a Beeman integrator with a 1 fs time step. Structures were saved every 0.1 ps. Five optimized structures were initially selected from previous simulated annealing results:⁴ str2, str4, str7, str8, and str9 and used in this work as initial structures. Among the low energy structures previously identified,⁴ these five were taken to ensure diversity in Dye–Arg and Trp–Arg relative orientations. For each starting structure, 5 ns trajectories were performed at 8 temperatures ranging from 150 to 500 K with a uniform step of 50 K. Since fluorescence lifetime is ca. 10 ns at 150 K and progressively drops down to ca. 2 ns at 465 K, a sampling time of 5 ns repeated for 5 different starting structures at each temperature appears to be adequate to capture the essentials of the dynamics underlying the quenching process.

2.4. Density Functional Theory Calculations. In order to gain more insight into the energy components that are crucial in shaping conformations where electron transfer is expected to be favorable, a conformation with stacked Dye and Trp rings was selected for refined quantum chemistry calculations at DFT level. We used the B3LYP functional augmented with an empirical term for dispersion^{21,22} with the SVP basis set for full geometry optimization, using the Turbomole software package.^{23,24} As for MD simulation, a B–N atom pair was replaced by two carbons. The structure was partitioned into components and the binding energy between these components was expressed as the sum of repulsion, electrostatic, orbital interaction and dispersion terms using a Morokuma–Ziegler type decomposition.¹³ This was applied to

four peptide fragmentation schemes in order to obtain a detailed picture of its local, intramolecular interactions. The calculations were performed at the B3LYP-D/TZ2P level with the ADF 2010.02 package.²⁵

3. PEPTIDE MOLECULAR DYNAMICS

3.1. Atom Labeling. Atomic ordering starts from the BODIPY which is at the N-termination of the peptide. Oxygen atoms of the linker are numbered from the dye to the peptide. As shown in Scheme 1, hydrogen bonds are designated by “H label”_“group name”_“heteroatom”_“group name”, e.g. H_W is the amino hydrogen in ϵ 1 position of the Trp side chain. HN_R is the peptidic HN of Arg while H_R corresponds to an HN of the Arg side chain. NH₂_cap stands for the NH₂ group linked to the C-terminus Trp residue. O_R stands for the Arg carbonyl oxygen, O_W the Trp carbonyl oxygen, O_Dye the oxygen in the BODIPY, O_L1 and O_L2 are on carbonyls of the linker closer and farther respectively to the BODIPY rings. O_P1 and O_P4 correspond to carbonyl oxygens of the first and the fourth Pro residues, respectively. NH₂_cap stands for a hydrogen of the Trp amide cap and HN_L1 stands for the HN in the first amide bond of the linker. The notation “2nd H_R” is used when a heteroatom is involved in two H-bonds with the Arg side chain.

3.2. Many-Body Effects. Fluctuations of the DyeX-(Pro)₄-Arg⁺-Trp conformations were calculated at 298 K with and without polarization included in AMOEBA to identify the role of many-body effects on trajectories. To switch off polarization, the values of the atomic polarizabilities were set to zero during the simulations, keeping all other parameters unchanged. The starting structure for each trajectory was initialized by a geometry optimization. The structures optimized with and without polarization are practically identical, having an RMSD value of 0.21 Å. Five simulations were performed for each case, each having a different set of initial velocities that were randomly generated. Care was taken to ensure that each of these five pairs of MD trajectories were completely independent. The final structure of each trajectory was reoptimized and the 5 structures for each case are shown superimposed in Figure 1. These superimposed structures were created using UCSF Chimera molecular graphics and analysis software.^{26,27} Chimera routines were used to generate sequence alignments and graphics of the two superimposed groups of five structures shown in Figure 1. The root-mean-square deviation (RMSD) of all atoms (excluding hydrogens) was averaged by Chimera²⁷ over the 10 pairs of five structures for each case. Structures calculated without polarization exhibited an RMSD = 0.819 Å, and those calculated with the polarizable force field showed an average RMSD = 0.106 Å. In the latter case limited dynamics of the linker generates limited disorder in the dye orientation (see Figure 1b). Figure 1a shows that without polarization, only the (Pro)₄-Arg segment remains somewhat rigid. This is expected for (Pro)₄ while it is the charge on Arg which likely makes it is less prone to large amplitude motion. On the other hand both the dye and Trp orientations fluctuate strongly, dominating the large increase in RMSD mentioned above. It is thus clear that polarization makes a considerable difference in the structural compactness for this singly protonated peptide. Many-body interactions could have significant consequences for a fluorescence quenching process such as electron transfer which depends exponentially on the separation between the dye and the Trp side chain and also the energetics associated with electrostatic interactions.

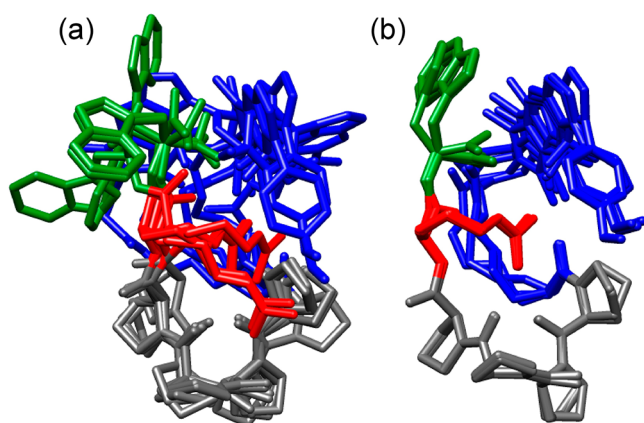


Figure 1. Structures of the peptide DyeX-(Pro)₄-Arg⁺-Trp calculated at 300 K by molecular dynamics using the AMOEBA force field. The dye (blue), tryptophan (green), arginine (red) and proline (gray) are indicated in (a) five superimposed structures calculated without polarization having a root mean standard deviation of RMSD = 0.819, and (b) five superimposed structures calculated with polarization having RMSD = 0.106.

3.3. Dye–Trp Proximity Analysis. The polyproline sequence is known to have significant backbone rigidity. In the present case, stiffness of the (Pro)₄ segment maintains its conformation during all trajectories from 150 to 500 K. Thus, according to its initial structure, a trajectory may generate some structures that others could not. The use of five different initial structures for molecular dynamics simulations at each temperature partly compensates for the bias introduced by trajectories which individually depend on their starting structure. At low temperatures, structures vibrate without leaving their initial potential wells. As the temperature increases, structural transitions are observed, leading to several new minima. The choice of starting structures utilized the sampling previously carried out.⁴ Structures str2 and str8 have similar (Pro)₄ conformations, whereas this segment is different for str7, str9, and str4. These are summarized in Tables 1 and 2, not starting structures, where each amide bond linkage is denoted as “t” for trans or “c” for cis. For str9, this difference also involves the first Proline residue and is the result of a rotation of ψ_{P1-P2} . The (Pro)₄ conformation in str7 differs by a rotation of the ω

Table 1. Description of Selected Structures of Type str2^a

structural property	str2_400 K_1728	str2_400 K_3187	str2_400 K_3484	str2_400 K_4235
Dye–Trp (Å)	5.17	6.59	6.72	3.93
Dye and Trp parallel	yes	yes	no	yes
Trp position	exo	endo	endo	endo
Arg side chain hydrogen bonds	3	3	3	3
(Pro) ₄ hydrogen bonds	2	2	2	3
(Pro) ₄ amide dihedrals $\omega 1-\omega 4$	t-t-c-t	t-t-c-t	t-t-c-t	t-t-c-t
N P1–CO P4 distance (Å)	7.69	9.08	7.47	7.08

^aValues are measured using geometries optimized at the AMOEBA level. Dye and Trp are considered to be parallel when $|\cos(\text{Dye}/\text{Trp})| > 0.9$. (Pro)₄ amide dihedrals are numbered from the O_{linker}-N_{P1} peptide bond to O_{P4}-N_{Arg} where P_n is the nth proline. A hydrogen bond is assumed to exist when the corresponding H...X distance is less than 2.5 Å.

Table 2. Description of Selected Structures of Types str4, str7, and str9^a

structural property	str4_all _0000	str4_500 K_4861	str7_400 K_1420	str7_400 K_4277	str9_400 K_1615
Dye–Trp (Å)	7.57	6.43	5.27	4.52	5.55
Dye and Trp parallel	no	no	no	yes	no
Trp position	exo	exo	exo	exo	exo
Arg side chain hydrogen bonds	4	2	5	5	4
(Pro) ₄ hydrogen bonds	3	0	2	2	2
(Pro) ₄ amide dihedrals $\omega 1-\omega 4$	t-t-t-t	t-t-t-t	c-t-c-t	c-t-c-t	t-t-c-t
N P1–CO P4 distance (Å)	9.16	11.15	7.16	6.72	9.32

^aValues are measured using geometries optimized at the AMOEBA level. Description of the table data is identical to Table 1.

dihedral angle of the amide bond between the linker and P₁. In str4, ω dihedrals are all trans leading to more extended (Pro)₄ segments. Therefore, trajectories starting from these various structures will explore different areas of the potential energy surface. A set of ten conformations with different local interactions of the Dye, Arg, and Trp and including some variations in the Pro₄ backbone conformation was selected from the MD trajectories, corresponding to potential energy plateaus. Four were taken from str2 and three from str7 since trajectories propagated from these two starting points presented a variety of conformers leading to Dye–Trp proximity. These structures are named according to the initial structure, the thermostat temperature and the time index in units of 1 ps of its trajectory (e.g., str2_400 K_1728 is the structure formed after a propagation of 1728 ps at 400 K starting from str2). Two structures were taken from the trajectory starting from str4 since it involves a different conformation for the (Pro)₄ segment. The description of structures in terms of hydrogen bonds (considered if distances are smaller than 2.5 Å) and π stacking between the Dye and Trp side chain is given in Tables 1 and 2. Two of these structures, illustrating cases where the Dye and Trp side chain are in proximity and nearly parallel, are displayed in Figure 5.

Steric hindrance between the side chains and electrostatic repulsion between carbonyl groups impose limitations on the number of hydrogen bonds between (Pro)₄ and the Arg side chain. In the DyeX-(Pro)₄-Arg⁺-Trp sequence, the (Pro)₄ segment “solvates” the protonated Arg side chain most of the time with two of its carbonyl groups. The (Pro)₄ conformation fluctuates with little consequence, except for exchanging two Pro carbonyls in the Arg side chain solvation. Structural transitions principally concern the peptide terminations: Trp side chain at the C terminus and the Dye at the N terminus, which is attached by a linker that has high flexibility. As the peptide is globularly structured around the Arg side chain, the linker primarily allows the peptide to be more or less compact, eventually leading to structures in which the Trp side chain is free enough to move inside the globular structure. Thus, the Trp side chain is quite mobile and can be either hindered in an internal position or move freely outside the globular structure. Because of this high flexibility, the Trp side chain can occasionally form a hydrogen bond with the first Pro residue while the Trp NH₂ cap can bind to the carbonyl of the fourth

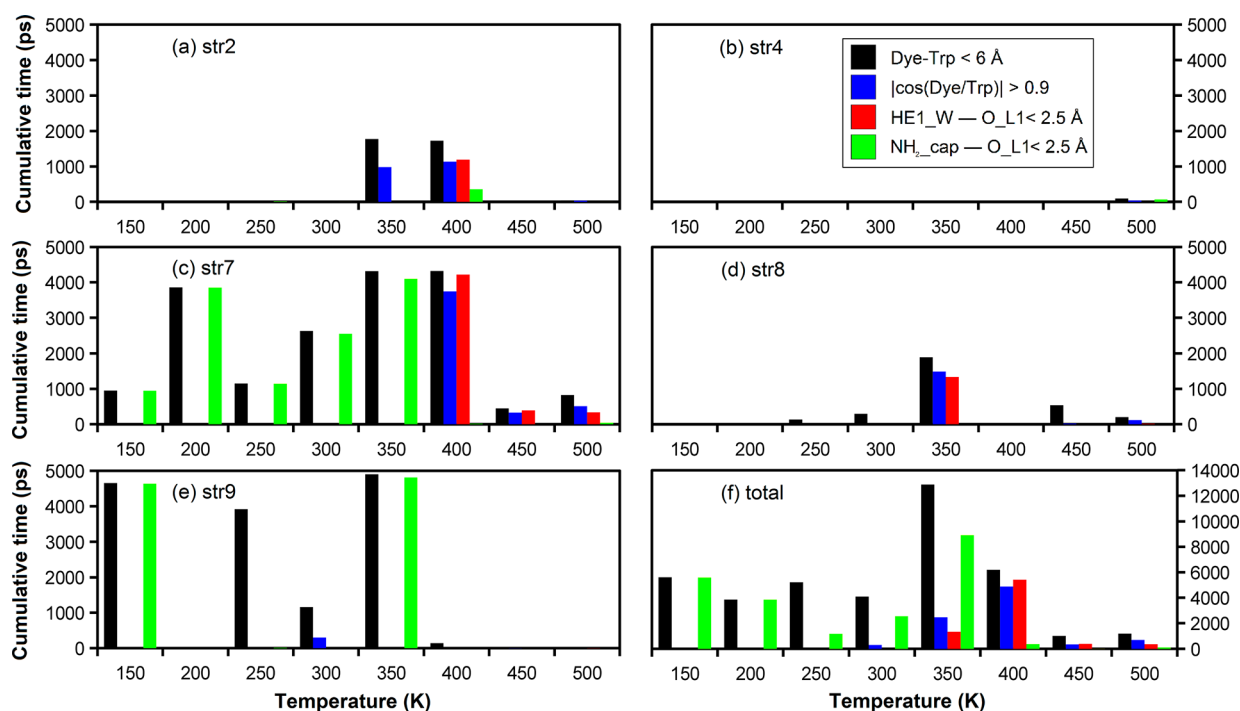


Figure 2. Dye–Trp proximity occurrence and correlation with geometry in molecular dynamics trajectories starting from structures (a) str2, (b) str4, (c) str7, (d) str8, (e) str9, and (f) the total occurrence for the 5 trajectories at each temperature, from 150 to 500 K. Proximity is considered for Dye–Trp distance < 6 Å and O_L1 is considered to be involved in H-bond with either H_W or NH₂_cap if the distance between the two atoms is below 2.5 Å.

Pro residue which is nearer in the peptide sequence or with the carbonyl of Arg that is even closer and usually available. NH- π interactions can also occur between the cap and the aromatic group of the Dye.

The (Pro)₄ conformation not only limits possible relative positions of the Dye, Trp and Arg residues, it also changes hydrogen bonds which may be formed between Pro oxygens and N–H hydrogen atoms of Arg and Trp. We have shown the importance of these hydrogen bonds in forming a stacked conformation. Therefore, if electron transfer involves a π -stacking between the Dye and Trp, then the (Pro)₄ conformation similar to that in str2 may be needed for a quenching interaction to occur. Electron transfer can be achieved between the Trp side chain and the Dye for a separation greater than 8 Å. However, at such a distance, the Dye and Trp are not necessarily interacting directly with each other, since the Arg side chain is able to insert in between them. As a consequence, direct correlation between the positions of the Dye and Trp can be identified meaningfully only at short separations. A separation distance criterion of 6 Å was found to allow for an important cumulative time of Dye–Trp proximity, while avoiding a bad correlation due to conformers having the Arg side chain between Dye and Trp. In the following we concentrate on the analysis of various types of structures in which the Dye and Trp side chain are in this distance range, because of their likely relevance to fluorescence quenching.

For each trajectory, the cumulative time for which the structure corresponds to a Dye–Trp separation less than 6 Å is shown in Figure 2 (black thick lines). The dihedral angle has been calculated between the BODIPY 3-rings and the Trp side chain. When these two chemical groups are parallel, the cosine of their relative dihedral angle is either lower than -0.9 or greater than $+0.9$, depending on their relative position (blue

thick lines). The presence of the H_W–O_L1 or NH₂_cap–O_L1 H-bonds is indicated by the red and green thick lines in Figure 1. A hydrogen bond is assumed to exist when the corresponding H...X distance is less than 2.5 Å. The H-bond, H_W–O_L1, links the Trp side chain HN and the carbonyl of the linker nearest to the BODIPY rings. NH₂_cap–O_L1 stands for the H-bond including the same oxygen atom bound to a hydrogen of the Trp amide cap. The presence of these H-bonds shows a strong dependence upon starting structure, e.g., trajectories propagated from str4 exhibit a Dye–Trp separation < 6 Å only in the 500 K trajectory and for short time durations. When Dye and Trp are separated by less than 6 Å, O_L1 is linked almost always to H_W or to the NH₂_cap. Such H-bonds dock these two groups together, an interaction favorable to Dye–Trp proximity. For some trajectories Dye–Trp proximity can be correlated with parallel Dye–Trp ring structures. This correlation is especially high for trajectories starting from str7 at temperatures greater than 350 K and is important for trajectories from str2 at 350 and 400 K and str8 at 350 K. Although H-bonds between the Arg side chain and Pro oxygens precondition the backbone structure of the molecule, they do not appear to be strongly correlated with Dye–Trp relative positions.

3.4. Correlated H-Bonds. Dye–Trp relative position is a key issue for the understanding of the structure–quenching relationship. For each of Figures 3 and 4, four panels are included: (a) total potential energy, (b) cosine of Dye–Trp dihedral angle, (c) Dye–Trp separation, and (d) hydrogen bond distances. The evolution of both Dye–Trp separation and cosine of Dye–Trp dihedral angle is discussed for several of the 40 calculated trajectories. Their profiles are compared to hydrogen bond distances and potential energy. All energetics,

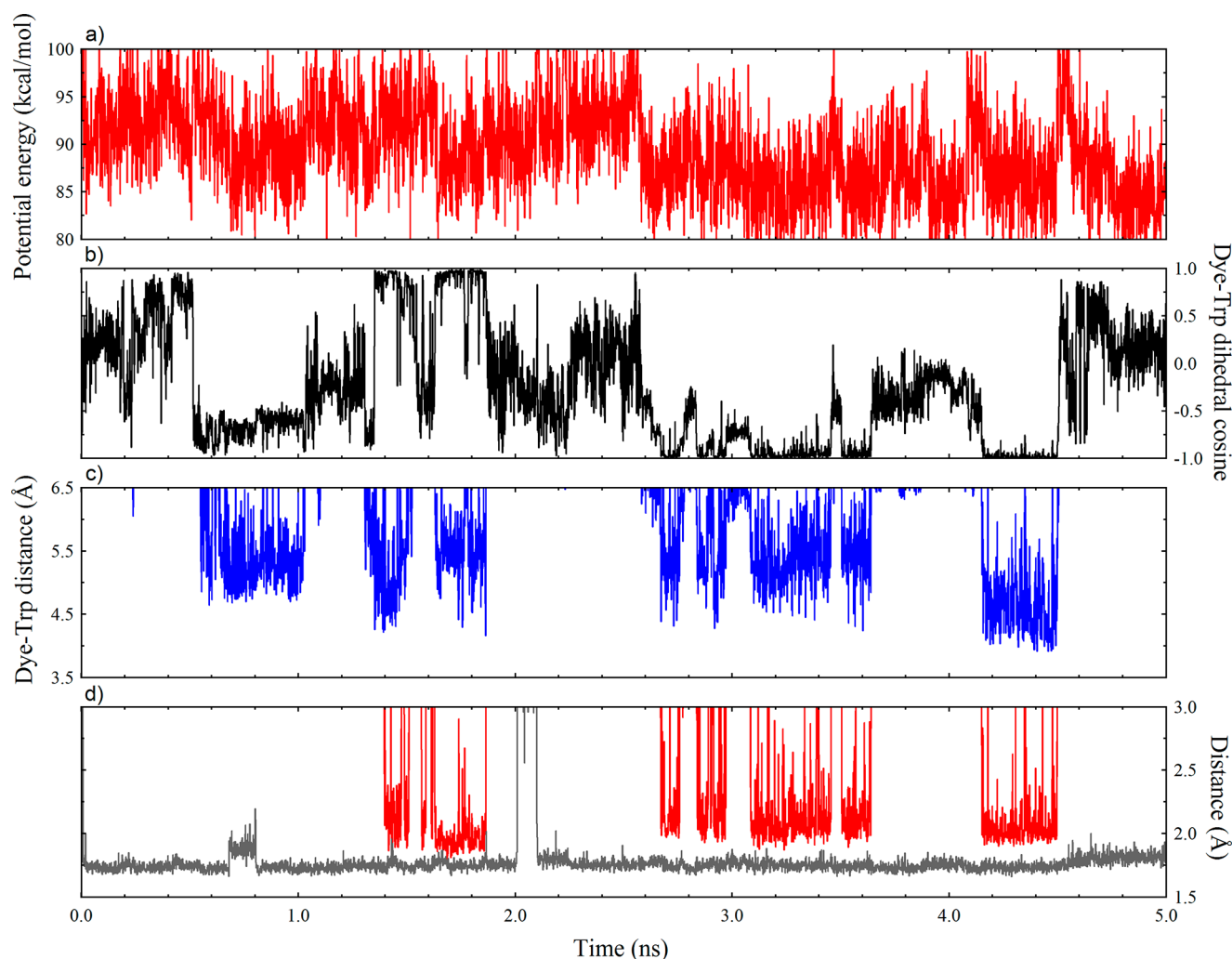


Figure 3. Analysis of trajectory str2 at 400 K. Evolution as a function of time (0–5 ns) of (a) total potential energy, (b) cosine of Dye–Trp dihedral angle, (c) Dye–Trp distance, and (d) distances of hydrogen bonds H_W–O_{L1} (red) and H_R–O_{Dye} (gray); see section 3.1 for details.

dihedral angles and distances present in the plots are averages performed for every ps of the trajectories.

For str2, at 400 K (Figure 3) as well as at lower temperatures, the Arg side chain is H-bonded to OCH₃ most of the time (H_R–O_{Dye}). Several proximity plateaus (<6 Å) are observed in Figure 3(c) for the Dye–Trp separation distance. Each of these plateaus corresponds to structures with parallel rings of the Dye and Trp side chain in Figure 3b. These periods are strongly correlated with an H-bond (red curve in Figure 3d) coupling the Trp side chain HN to linker's first oxygen (O_{L1}). Even though this condition is not sufficient to form parallel rings, it is also fulfilled for the first period of proximity. As a consequence, the other possible hydrogen bonds made by Trp HE1, to O_{L2} and to O_{P1}, do not show significant correlation with the Dye–Trp distance. As observed in Figure 3a, Dye–Trp proximity plateaus correspond to relatively low potential energy conformers.

Dynamics of str7 at 400 K (see Figure S5 in the Supporting Information) involves a stronger correlation than observed for str2 between Dye–Trp proximity (<6 Å), the dihedral angles and the H-bond between H_W and O_{L1}. Between 2.85 and 3.2 ns, this H-bond is broken and both Dye–Trp proximity and parallelism of Dye and Trp rings are lost. Corresponding structures are higher in potential energy by more than 5

kcal·mol^{−1}. Both before and after this time interval, H_W is less tightly attached to O_{L2} than it is to O_{L1}.

For str8 at 350 K (see Figure S6, Supporting Information), during the time interval 0.5 to 1.85 ns, Dye–Trp ring parallelism for a separation distance <5.5 Å is correlated with the formation of H-bonds H_W–O_{L1}. Additional periods of reduced proximity are correlated with the dihedral angle. Between 2.6 and 4.38 ns, middle range proximity (~5.5 to 6.5 Å) can be observed. This period of middle range proximity is less correlated to Dye–Trp dihedral angle and hydrogen bonds than the Dye–Trp proximity plateau <5.5 Å. Finally, from 3.7 to 4.3 ns, the Dye and Trp rings tend to be more parallel, their relative proximity is slightly increased involving insignificant modification in the H-bond network.

For trajectories starting from str9 at 150 K shown in Figure 3 and 350 K (see Figure S7), three hydrogen bonds are observed to be correlated with the Dye–Trp proximity for almost the entire trajectories: NH₂–cap–O_{L1} (yellow), H_R–O_{Dye} (dark gray) and H_R–O_W (vegas gold). These 150 and 350 K trajectories correspond to a peptide that is trapped most of the time in a single potential well. However trajectories at intermediate temperatures show different dynamics as shown in Figure 2e. Consequently, an increase in kinetic energy does not guarantee that the peptide will overcome the potential barrier

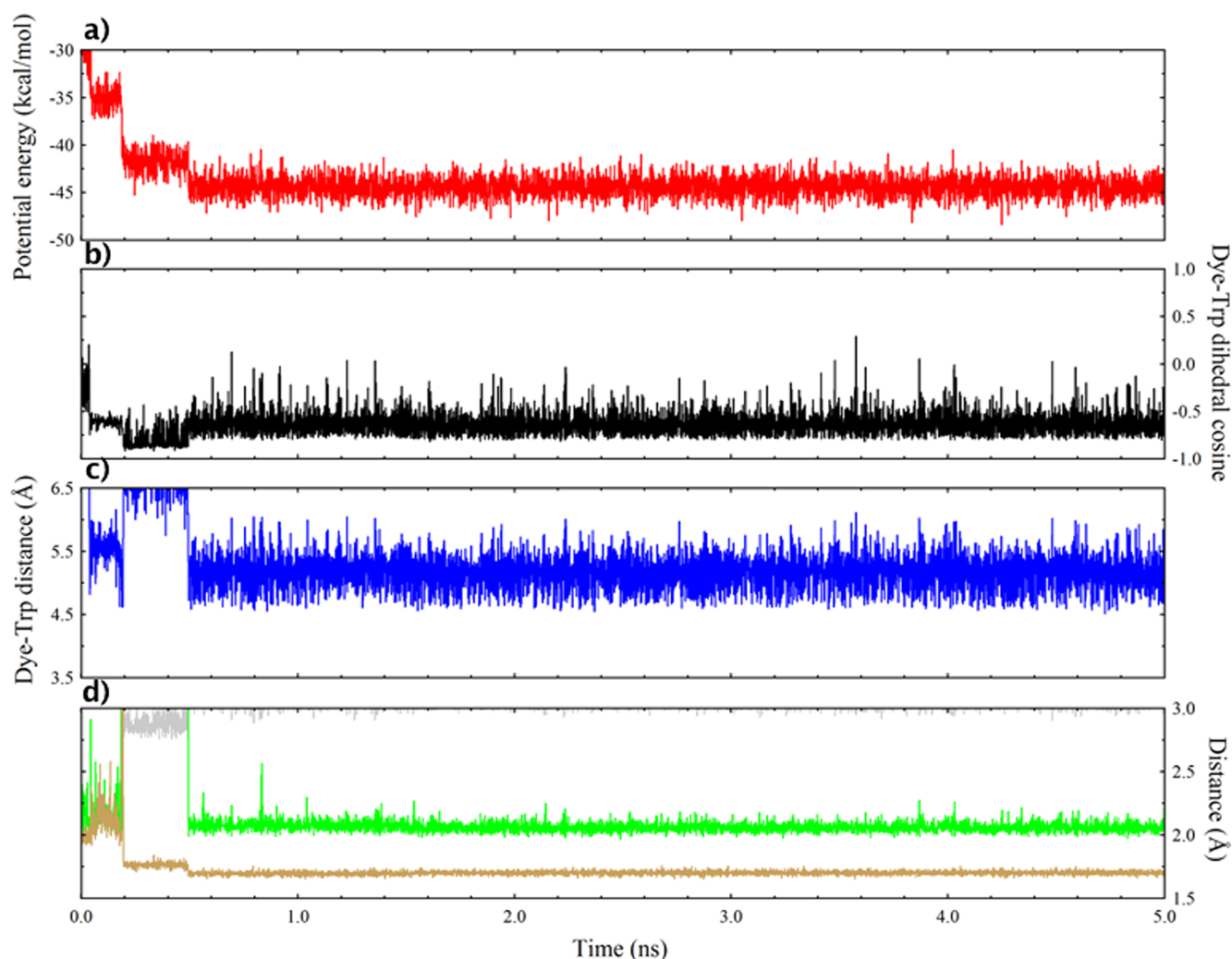


Figure 4. Analysis of trajectory str9 at 150 K. Evolution as a function of time (0–5 ns) of (a) total potential energy, (b) cosine of Dye–Trp dihedral angle, (c) Dye–Trp distance, and (d) distances of hydrogen bonds H_R-O_Dye (gray), NH₂_cap-O_L1 (green) and H_R-O_W (brown); see section 3.1 for details.

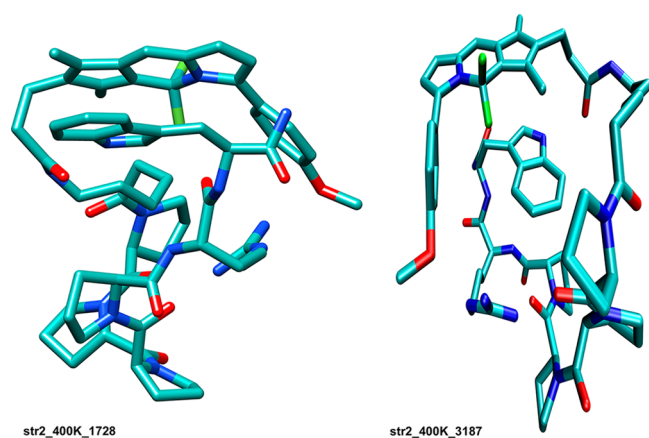


Figure 5. Two str2-type structures, str2_400 K_1728 and str2_400 K_3187, illustrating cases in which the Dye and Trp side chain planes are nearly parallel. Their main difference lies in the orientation of the Trp side chain relative to the peptide backbone.

formed by electrostatic, polarization, and dispersive interactions.

4. ANALYSIS OF BINDING INTERACTIONS

DFT calculations using the B3LYP-D functional were performed to identify the dominant interactions in a structure involving Dye–Trp proximity, in order to provide deeper understanding of the local interactions and thus delineate the requirements for future force field modeling of such systems.

4.1. Quantum Chemical Level. Structures in which the Dye and Trp side chains are close to one another are particularly relevant to electron transfer. Among these, structures involving proximate Dye and Trp indole with parallel orientations may allow for the closest possible approach and be relevant to short-range electron transfer. It is thus important to understand the nature of the interactions which influence the shaping of such conformations. Structure str2_400 K_1728 (see Figure 5) was selected among those described in Tables 1 and 2, as the one in which such π -stacking is associated with the smallest possible Dye–Trp distance, corresponding to a plateau of relatively stable structures (see Figure 3). Its internal energetics was then investigated in detail at the DFT level.

The Morokuma–Ziegler type decomposition¹³ amounts to breaking the interaction energy between two molecular units into repulsion, electrostatic, orbital interaction and dispersion

terms if a dispersion-corrected functional is used. Note that polarization is included in the orbital interaction term, together with stabilization due to orbital overlap including charge transfer, and also participates in the electrostatic term. As a result, direct comparison of this decomposition with the force field energy components cannot be straightforward.

This decomposition procedure is usually applied to intermolecular interactions. It can be extended to intramolecular interactions by defining fragments within a single molecule and it is this latter use that is relevant here. Since each energy term pertains to the entire group of fragments, we define four models in order to focus on the role of hydrogen bonds, charged Arg side chain and π -stacking between the Dye and Trp side chain in each energy term. Four models of decreasing complexity have been used for the purpose of energy decomposition:

- **Dye/Arg–Trp** (Figure 6a). The Dye (on the right) is terminated by a methyl group after the first linker amide

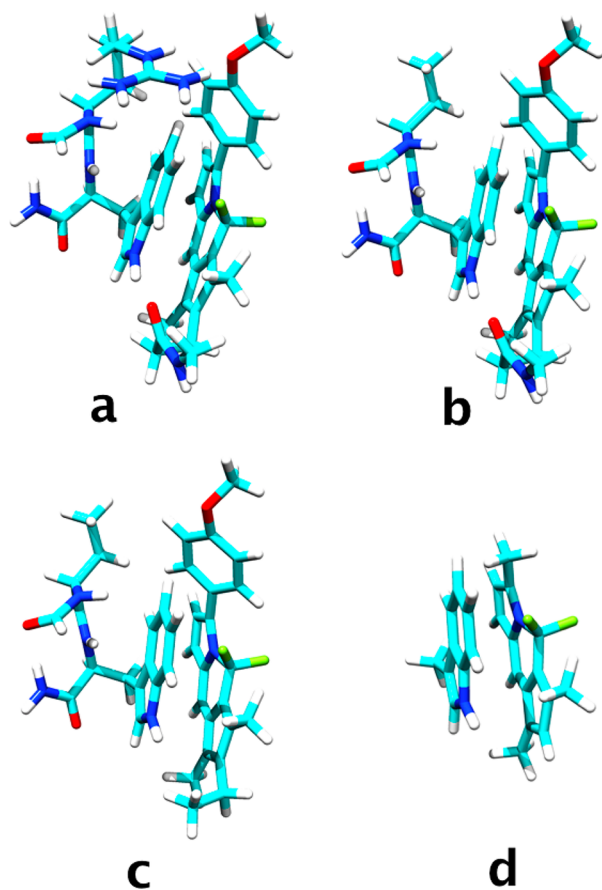


Figure 6. Models of the Dye/Arg–Trp fragment from structure str2_400 K_1728 used in the decomposition of the binding energy. (a) Dye/Arg–Trp, (b) Dye/Trp, (c) Dye/Trp without H bond, and (d) unsubstituted Dye/Trp side chain.

bond and the Arg N-terminus (upper left) is followed by a CHO group. Here, the Arg and Trp are considered together as a single fragment. This model amounts to eliminating the linker and the (Pro)₄ segment.

- **Dye/Trp** (Figure 6b). The Arg side chain of the previous model is truncated at C _{β} and replaced by a methyl group. This results in a neutral system and eliminates the

hydrogen bond between the Arg side chain and the Dye ether oxygen.

- **Dye/Trp without H bond** (Figure 6c). The previous model is simplified by replacing the amide linker by a methyl group; thereby eliminating the hydrogen bond of the indole N–H of Trp (H_W–O_L1).
- **Unsubstituted Dye/Trp side chain** (Figure 6d). Substituents of both the Trp indole and BODIPY rings are replaced by methyl groups; thus focusing on aromatic–aromatic ring interactions only.

The energy decomposition results are displayed in Table 3. The largest model, Dye/Arg–Trp (Figure 6a), demonstrates that very strong interactions exist between the Dye and Arg–Trp fragments with a total interaction energy of $-51 \text{ kcal}\cdot\text{mol}^{-1}$. This is composed of a large Pauli repulsion term and of large electrostatic, orbital interaction and dispersion stabilizing terms, none of which is sufficiently dominant to provide a reasonable description of the stabilizing driving force by itself. The Arg charge, the ionic hydrogen bond between the Arg side chain and the ether oxygen, and the neutral H_W–O_L1 hydrogen bond generate large electrostatic and orbital interaction components of -46.7 and $-28.5 \text{ kcal}\cdot\text{mol}^{-1}$, respectively, amounting together to 43% of the interaction energy (see Table 3).

Smaller models involve a reduced number of atomic interactions, leading to smaller energy terms. The models are designed to eliminate interactions in a stepwise manner. It is therefore useful to consider how each energy term changes in the sequence of successively smaller models.

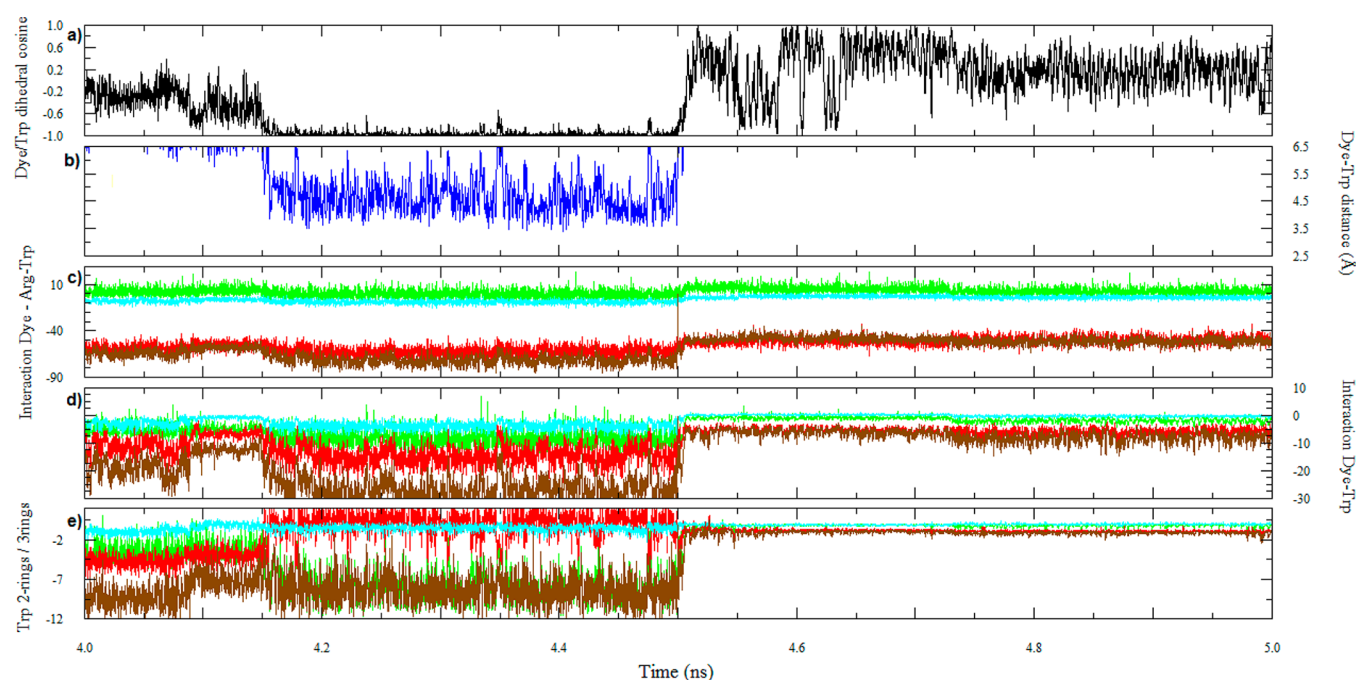
In the absence of Arg, (Dye/Trp model, Figure 6b), there is one less hydrogen bond and the system is neutral. The total binding energy is significantly reduced, demonstrating the importance of these two effects. Electrostatics and orbital interactions are strongly diminished, decreasing to 35% of the interaction energy. Dispersion is only slightly reduced, resulting in an increased percentage of the interaction energy. Size reduction of the model also leads to reduced repulsion. Removing the H_W–O_L1 hydrogen bond (Figure 6c) leads to a much smaller decrease of the binding energy, as expected for a neutral hydrogen bond. Significant decreases of both electrostatic and orbital terms are revealing the crucial role of hydrogen bonds in the formation of the ring-interaction conformation by constraining the separation of the Dye and Trp. Because of these decreased terms, dispersion becomes the dominant stabilizing term. Finally, simplification of the Dye into its three rings and of Trp into its indole side chain leads to a system (Figure 6d) without hydrogen bonds and polarization contributions from the Arg formal charge. The resulting binding energy depends completely on aromatic–aromatic ring interactions. The results in Table 3 clearly show that in such a structure, the primary driving force for bringing the two groups of cycles into proximity is the dispersion interaction.

These results demonstrate that Dye, Trp, and Arg hydrogen bonds and Arg charge interactions provide the dominant contributions to binding energy for structures involving Dye and Trp proximity less than 6 Å, such as str2_400 K_1728. The local Dye–Trp interaction is primarily dispersive.

4.2. Molecular Mechanics Level. Energy decomposition is of course also possible at the force field level. AMOEBA energies were decomposed into electrostatic, polarization and van der Waals terms. Electrostatics is computed as the sum of atom–atom interactions of multipoles—charges, dipoles, and

Table 3. Decomposition of the Binding Energy into Components for the Models Shown in Figure 6, Computed at the B3LYP-D/TZ2P Level^a

energy term	Dye/Arg-Trp	Dye/Trp	Dye/Trp without H bond	unsubst Dye/Trp side chain
total binding energy	−51.0	−27.0 (−24.0) ^b	−18.0 (−9.0) ^c	−8.3 (−9.7) ^d
repulsion (Rep)	61.7	50.2 (−11.5) ^b	36.1 (−24.1) ^c	31.9 (−4.2) ^d
electrostatic	−46.7	−29.4 (−17.3) ^b	−15.5 (−13.9) ^c	−13.0 (−2.5) ^d
orbital interactions	−28.5	−15.2 (−13.3) ^b	−7.9 (−7.3) ^c	−5.9 (−2.0) ^d
dispersion (Disp)	−37.4	−32.5 (−4.9) ^b	−30.9 (−1.6) ^c	−21.3 (−9.6) ^d

^aEnergy differences between successive models are given in parentheses. ^bDifference in absolute value with that of the Dye/Arg-Trp model.^cDifference in absolute value with that of the Dye/Trp model. ^dDifference in absolute value with that of the Dye/Trp without H bond model.**Figure 7.** Analysis of trajectory str2 at 400 K between 4.0 and 5.0 ns. Evolution as a function of time of (a) cosine of Dye–Trp dihedral angle, (b) Dye–Trp distance (Å), (c–e) van der Waals (green), electrostatic (red) and polarization (cyan) components of the interaction energies and the total energy (brown) (kcal·mol^{−1}). Parts c–e of Figure 5 correspond to the Dye/Arg–Trp, Dye/Trp, and unsubstituted Dye/Trp side chain (Trp 2-rings/3 rings) models, respectively.

quadrupoles, summed over all pairs of atoms, one in each interacting fragment. Polarization is computed as the sum of multipole–induced dipole and induced dipole–induced dipole atomic interactions. The induced dipoles are those generated by the entire molecule, not just the fragments. It cannot be directly compared to any term in the DFT analysis, since it is distributed in the DFT electrostatics and orbital interactions. Finally the van der Waals component includes both attractive and repulsive contributions, another significant difference from DFT partitioning. The AMOEBA energy components can be further partitioned into local contributions. One of the previously described trajectories was used and energy components were extracted over a time period, for models analogous to Dye/Trp, Dye/Trp without H bond, and unsubstituted Dye/Trp side chain used above in the DFT analysis.

The 400 K dynamics starting with structure str2 was used since it shows a plateau of Dye–Trp proximity between 4.15 and 4.5 ns, with the Dye–Trp distance fluctuating between 4.3 and 6 Å and their two planes being essentially parallel. Results displayed in Figure 7 show that during this plateau, the total energy is dominated by a strong electrostatic stabilization of −50 to −70 kcal·mol^{−1} in the Dye/Arg–Trp model, with van

der Waals energy fluctuating around zero and a polarization contribution fairly stable near −10 kcal·mol^{−1}. Smaller models yield results which are fully consistent with DFT, indicating that elimination of Arg considerably reduces electrostatics, which decreases to nearly zero for the smallest model fragments. A van der Waals contribution in the −5 to −10 kcal·mol^{−1} range becomes the only significant term in the smallest model, Unsubstituted Dye/Trp side chain. Analysis of times beyond 4.5 ns indicates that all local interaction terms drop to nearly exactly zero because the Dye–Trp distance is larger than 8 Å. In the Dye/Arg–Trp model, the charge on Arg maintains large electrostatic components at all distances as it is only the type of charge solvation that is changing. On the other hand, the time period preceding the plateau has Dye–Trp distance in the 8 Å range, thus involving small but non negligible interaction terms.

The results described above indicate that hydrogen bonds may be crucial in stabilizing structures which allow the dye and Trp side chain to attain a proximity to one another. One of these hydrogen bonds connects the first amide oxygen in the linker to the HN bond in the Trp side chain. It may be hypothesized that the absence of this linker–amide group would make the Dye–Trp proximity less likely, or that the dye

would fluctuate more strongly even when Trp side chain is nearby.

5. CONCLUSIONS

Molecular dynamics simulations of the derivatized DyeX-(Pro)₄-Arg⁺-Trp peptide using the new generation AMOEBA force field yield a refined picture of the structural dynamics of this peptide as a function of temperature from 150 to 500 K. Although the number of independent starting structures are too few to allow for converged statistics, a clear picture emerges in which the structural rigidity provided by the (Pro)₄ segment permits interaction between the Dye and the indole side chain, often enough to make electron transfer to the photoexcited dye likely. A force field including many-body effects such as AMOEBA is required to account for the structural compactness of the peptide. While the local Dye–Trp interaction is mainly dispersive at short separations, driving the system toward such conformations is largely due to electrostatic interactions generated by the electric charge of protonated Arg, and to hydrogen bonds which are often established between a linker carbonyl oxygen and one of the capped Trp N–H bonds. This assignment is based on both structural analysis of all structures generated in the MD simulations and on energy decomposition analysis at both classical and quantum mechanical levels. The good agreement between AMOEBA and DFT indicates that the physically based energy terms of the force field allow for a sound description of the interactions in packed conformations, where accurate electrostatic, polarization and dispersion terms are required. It is probably the first time that such a detailed assessment of a force field is made for a system this large. Averages which can be extracted from the simulations at temperatures between 150 and 500 K can then be used to fit the experimental temperature dependence of fluorescence quenching rates in order to compare these data to the prediction of the Marcus model of electron transfer. The results of such an analysis are presented in the companion paper, part II.²⁸

■ ASSOCIATED CONTENT

■ Supporting Information

Additional figures related to (A) structures used for data in Tables 1 and 2 and (B) trajectory analyses for additional starting structures and temperatures and (C) a set of new AMOEBA parameters derived for the dye. This material is available free of charge via the Internet at <http://pubs.acs.org>.

■ AUTHOR INFORMATION

Corresponding Author

*E-mail: (C.C.) carine.clavaguera@polytechnique.fr; (G.O.) gilles.ohanessian@polytechnique.fr; (J.H.P.) parks@rowland.harvard.edu. Telephone: (C.C. and G.O.)(33) (0) 1 69 33 48 01; (J.H.P.) (617) 497-4653. Fax: (C.C. and G.O.) (33) (0) 1 69 33 48 03; (J.H.P.) (617) 497-4627.

Notes

The authors declare no competing financial interest.

■ ACKNOWLEDGMENTS

This work was granted access to the HPC resources of [CCRT/CINES/IDRIS] under the allocation x2011085107 made by GENCI (Grand Equipement National de Calcul Intensif).

■ REFERENCES

- (1) Iavarone, A. T.; Parks, J. H. *J. Am. Chem. Soc.* **2005**, *127*, 8606–8607.
- (2) Iavarone, A. T.; Patriksson, A.; Van der Spoel, D.; Parks, J. H. *J. Am. Chem. Soc.* **2007**, *129*, 6726–6735.
- (3) Iavarone, A. T.; Duft, D.; Parks, J. H. *J. Phys. Chem. A* **2006**, *110*, 12714–12727.
- (4) Shi, X.; Duft, D.; Parks, J. H. *J. Phys. Chem. B* **2008**, *112*, 12801–12815.
- (5) Shi, X.; Parks, J. H. *J. Am. Soc. Mass Spectrom.* **2010**, *21*, 707–718.
- (6) Ren, J. W.; Ponder, P. J. *Comput. Chem.* **2002**, *23*, 1497–1506.
- (7) Rasmussen, T. D.; Ren, P.; Ponder, J. W.; Jensen, F. *Int. J. Quantum Chem.* **2007**, *107*, 1390–1395.
- (8) Ponder, J. W. *TINKER—Software Tools for Molecular Design*, Version 5.0 2008.
- (9) Ponder, J. W.; Ren, P. *J. Phys. Chem. B* **2003**, *107*, 5933–5947.
- (10) Ponder, J. W.; Wu, C.; Ren, P.; Pande, V. S.; Chodera, J. D.; Schnieders, M. J.; Haque, I.; Mobley, D. L.; Lanbrecht, D. S.; DiStasio, R. A., Jr.; et al. *J. Phys. Chem. B* **2010**, *114*, 2549–2564.
- (11) Ren, P.; Wu, C.; Ponder, J. W. *J. Chem. Theory Comput.* **2011**, *7*, 3143–3161.
- (12) Jensen, F.; Kaminský, J. *J. Chem. Theory Comput.* **2007**, *3*, 1774–1788.
- (13) Bickelhaupt, F. M.; Baerends, E. J. *Kohn-Sham Density Functional Theory: Predicting and Understanding Chemistry*. In *Reviews in Computational Chemistry*; Boyds, D. B., Ed.; Wiley-VCH: New York, 2000; Vol. 15, pp 1–86.
- (14) Semrouni, D.; Ohanessian, G.; Clavaguera, C. *Phys. Chem. Chem. Phys.* **2010**, *12*, 3450–3462.
- (15) Applequist, J.; Carl, J. R.; Fung, K.-K. *J. Am. Chem. Soc.* **1972**, *94*, 2952–2960.
- (16) Thol  , B. T. *Chem. Phys.* **1981**, *59*, 341–350.
- (17) (a) Riley, K. E.; Pitonak, M.; Jurecka, P.; Hobza, P. *Chem. Rev.* **2010**, *110*, 5023–5063. (b) Semrouni, D.; Clavaguera, C.; Dognon, J. P.; Ohanessian, G. *Int. J. Mass Spectrom.* **2010**, *297*, 152–161.
- (18) Halgren, T. A. *J. Am. Chem. Soc.* **1992**, *114*, 7827–7843.
- (19) Stone, A. J. *Chem. Phys. Lett.* **1981**, *83*, 233–239.
- (20) Stone, A. J. *Distributed Multipole Analysis for Gaussian Wavefunctions*, Version 2.2.03 2007.
- (21) Grimme, S. *J. Comput. Chem.* **2004**, *25*, 1463–1473.
- (22) Grimme, S. *J. Comput. Chem.* **2006**, *27*, 1787–1799.
- (23) Ahlrichs, R.; Bar, M.; Haser, M.; Horn, H.; Kolmel, C. *Chem. Phys. Lett.* **1989**, *162*, 165–169.
- (24) TURBOMOLE V6.2 2010, a development of University of Karlsruhe and Forschungszentrum Karlsruhe GmbH, 1989–2007, TURBOMOLE GmbH, since 2007; available from <http://www.turbomole.com>.
- (25) ADF2010.02, SCM, Theoretical Chemistry, Vrije Universiteit: Amsterdam, The Netherlands; available from <http://www.scm.com>.
- (26) Pettersen, E. F.; Goddard, T. D.; Huang, C. C.; Couch, G. S.; Greenblatt, D. M.; Meng, E. C.; Ferrin, T. E. *J. Comput. Chem.* **2004**, *25*, 1605–1612.
- (27) Meng, E. C.; Pettersen, E. F.; Couch, G. S.; Huang, C. C.; Ferrin, T. E. *BMC Bioinformatics* **2006**, *7*, 339–348.
- (28) Parks, J. H.; Semrouni, D.; Clavaguera, C.; Ohanessian, G. *J. Phys. Chem. B* **2013**, DOI: 10.1021/jp3078437.